

Supporting Information

Anthraquinone Derivatives Affording n-Type Organic Thin Film Transistors

**Masashi Mamada,^a Jun-ichi Nishida,^a
Shizuo Tokito^b and Yoshiro Yamashita*^a**

^aDepartment of Electronic Chemistry, Interdisciplinary Graduate School of Science and Engineering, Tokyo Institute of Technology, Nagatsuta, Midori-ku, Yokohama 226-8502, *Japan.*

^bNHK Science and Technical Research Laboratories, Kinuta, Setagaya-ku, Tokyo 157-8510, *Japan.*

E-mail: yoshiro@echem.titech.ac.jp

Contents

1. Syntheses
2. UV-vis absorption spectra
3. Differential pulse voltammogram
4. DFT calculations
5. X-ray analyses
6. XRD patterns
7. AFM measurements
8. Device fabrications
9. FET characteristics
10. I_D - V_D and I_D - V_G characteristics
11. References

General

Melting points were obtained on a SHIMADZU DSC-60. ^1H -NMR spectra were recorded on a JEOL JNM-ECP 300 spectrometer and referenced to the residual solvent proton resonance. EI mass spectra were collected on a JEOL JMS-700 mass spectrometer. IR spectra were recorded as KBr discs on a PERKIN ELMER FT-IR Spectrometer PARAGON 1000 spectrophotometer. Elemental analyses were performed at the Tokyo Institute of Technology, Chemical Resources Laboratory. UV-vis spectra were recorded on a SHIMADZU Multi Spec-1500. Differential pulse voltammograms were recorded on a HOKUTODENKO HZ-5000 containing terabutylammonium hexafluorophosphate (TBAPF₆) (0.1 mol dm⁻³ in dry dichloromethane). The Pt disk, Pt wire and SCE were used as working, counter, and reference electrodes, respectively. MO calculations were carried out by DFT methods at the B3LYP/6-311G(d) level using the Gaussian program. X-ray diffraction (XRD) measurements were carried out with a JEOL JDX-3530 X-ray diffractometer system. XRD patterns were obtained using Bragg-Brentano geometry with CuK α 5 radiation as an X-ray source with an acceleration voltage of 40 kV and a beam current of 30 mA. AFM experiments for films in tapping mode were performed using a SII NanoTechnology SPA-400 (DFM) instrument.

1. Syntheses

Materials.

Tetrakis(triphenylphosphine)palladium(0), *n*-butyllithium in *n*-hexane, THF and toluene were purchased from Kanto Chemicals and used without further purification. Tributylstannyll chloride was purchased from Wako Co. and used without further purification.

2,6-Diaminoanthraquinone and 4-trifluoromethylphenyl boronic acid were prepared according to the reported methods.^{1,2} 2-Bromo-5-(4-trifluoromethylphenyl)thiophene and 5-bromo-2-(4-trifluoromethylphenyl)thiazole were synthesized according to the reported methods³ and the stannylation reactions were carried out by a usual procedure that used *n*-BuLi and tributylstannyll chloride.

2,6-Bis(4-trifluoromethylphenyl)anthraquinone (1)

2,6-Dibromoanthraquinone (1.02 g, 2.78 mmol), 4-trifluoromethylphenyl boronic acid (1.06 g, 5.58 mmol), toluene (30 ml), tetrakis(triphenylphosphine)palladium(0) (0.143 g), potassium carbonate (1.67 g, 12.1 mmol) and water (30 ml) were added to a one-neck flask and the mixture was refluxed for 24 h. The reaction mixture was cooled to room temperature and filtered. The yellow residue was washed with water and dried. The product was purified by sublimation to give **1** (0.446 g, 32.4 %) as pale yellow crystals. mp 319–321 °C. $^1\text{H-NMR}$ (300MHz; CDCl_3 ; Me_4Si) δ (ppm): 8.59 (d, $^3J=1.8\text{Hz}$, 2H), 8.47 (d, $J=8.4\text{Hz}$, 2H), 8.07 (dd, $^3J_1=1.8\text{Hz}$, $J_2=8.4\text{Hz}$, 2H), 7.87 (d, $J=8.4\text{Hz}$, 4H), 7.80 (d, $J=8.4\text{Hz}$, 4H). The $^{13}\text{C-NMR}$ could not be taken due to the low solubility. MS/EI (70 eV): m/z 496 (M^+ , 100 %), 468 (14.21), 440 (8.95), 248 (7.06). IR (KBr) $\nu_{\text{max}}/\text{cm}^{-1}$: 1668 (CO), 1595, 1422, 1396, 1324, 1181, 1160, 1115, 1072, 1016, 953, 837, 720, 611. Anal. Calcd. For $\text{C}_{28}\text{H}_{14}\text{F}_6\text{O}_2$: C, 67.75; H, 2.84; F, 22.96; O, 6.45. Found: C, 67.61; H, 2.58.

2,6-Bis[5-(4-trifluoromethylphenyl)thiophene-2-yl]anthraquinone (2)

2,6-Dibromoanthraquinone (1.34 g, 3.67 mmol), 2-tributylstanny-5-(4-trifluoromethylphenyl)thiophene (3.86 g, 7.46 mmol), toluene (100 ml) and tetrakis(triphenylphosphine)palladium(0) (0.097 g) were added to a one-neck flask and the mixture was refluxed for 24 h. The reaction mixture was cooled to room temperature and filtered. The red residue was washed with hexane and dried. The product was purified by sublimation to give **2** (1.69 g, 69.6 %) as red crystals. mp 346–348 °C. The $^1\text{H-NMR}$ and $^{13}\text{C-NMR}$ could not be taken due to the low solubility. MS/EI (70 eV): m/z 660 (M^+ , 100 %), m/z 641 (4.45, $[\text{M}-\text{F}]^+$), m/z 330 (9.08). IR (KBr) $\nu_{\text{max}}/\text{cm}^{-1}$: 1668 (CO), 1590, 1445, 1415, 1322, 1301, 1176, 1124, 1064, 1012, 928, 840, 799, 741. Anal. Calcd. For $\text{C}_{36}\text{H}_{18}\text{F}_6\text{O}_2\text{S}_2$: C, 65.45; H, 2.75; F, 17.25; O, 4.84; S, 9.71. Found: C, 65.62; H, 2.61; S, 9.65.

2,6-Bis[2-(4-trifluoromethylphenyl)thiazol-5-yl]anthraquinone (3)

Anthraquinone derivative **3** was synthesized in 61.1 % yield by the similar method for **2**. Yellow crystals; mp 378–381 °C. The $^1\text{H-NMR}$ and $^{13}\text{C-NMR}$ could not be taken due to the low solubility. MS/EI (70 eV): m/z 662 (M^+ , 100 %), m/z 643 (6.51, $[\text{M}-\text{F}]^+$), m/z 491 (14.65, $[\text{M}-\text{CF}_3\text{PhCN}]^+$), m/z 320 (22.44, $[\text{M}-(\text{CF}_3\text{PhCN})_2]^+$). IR (KBr) $\nu_{\text{max}}/\text{cm}^{-1}$: 1674 (CO), 1592, 1427, 1403, 1321, 1163, 1138, 1107, 1066, 1014, 938, 845, 744, 633. Anal. Calcd. For $\text{C}_{34}\text{H}_{16}\text{F}_6\text{O}_2\text{N}_2\text{S}_2$: C, 61.63; H, 2.43; F, 17.2; O, 4.83; N, 4.23; S, 9.68. Found: C, 61.35; H, 2.21; N, 4.23; S, 9.53.

2. UV-vis absorption spectra

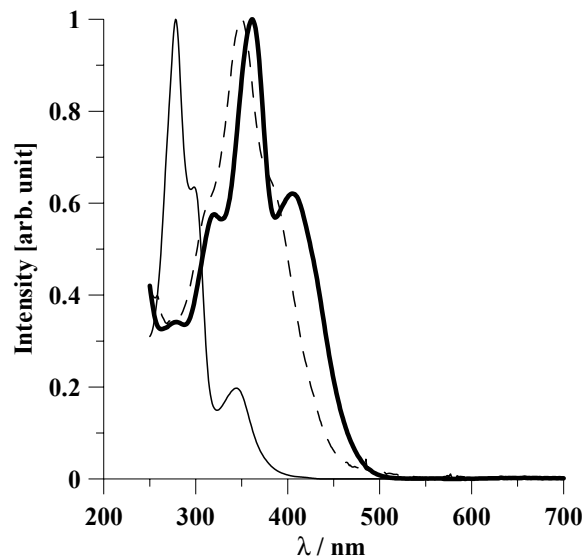


Figure S1. Absorption spectra of **1** (thin solid line), **2** (thick solid line) and **3** (dashed line) in dichloromethane solution.

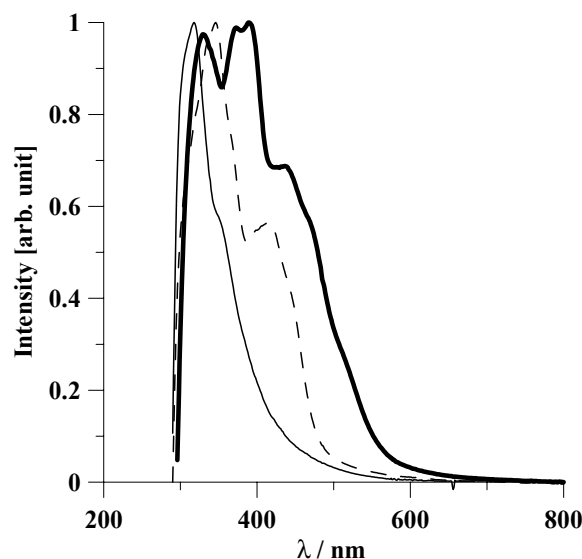


Figure S2. Absorption spectra of **1** (thin solid line), **2** (thick solid line) and **3** (dashed line) in film.

3. Differential pulse voltammogram

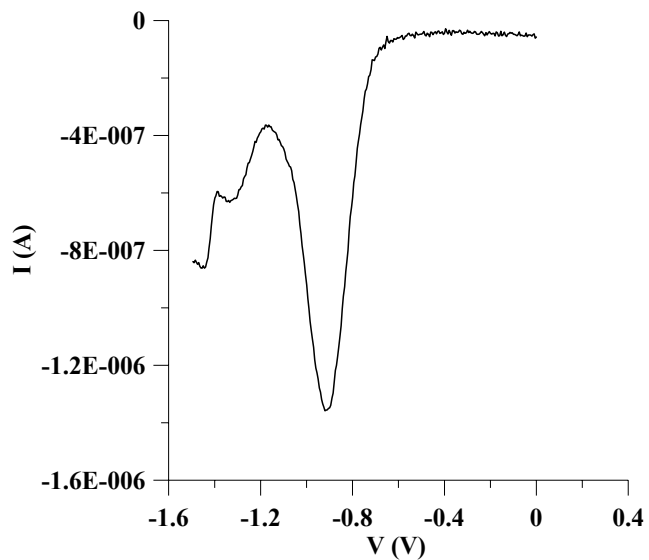


Figure S3. Differential pulse voltammogram of **1**.

4. DFT calculations

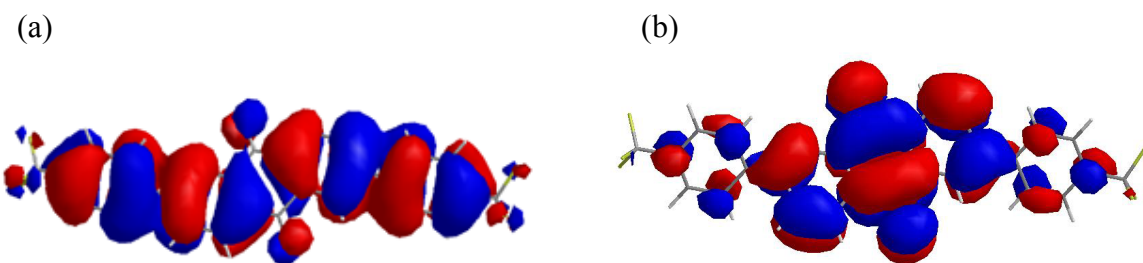


Figure S4. (a) HOMO orbital (-7.13 eV) and (b) LUMO orbital (-3.31 eV) of **1**.

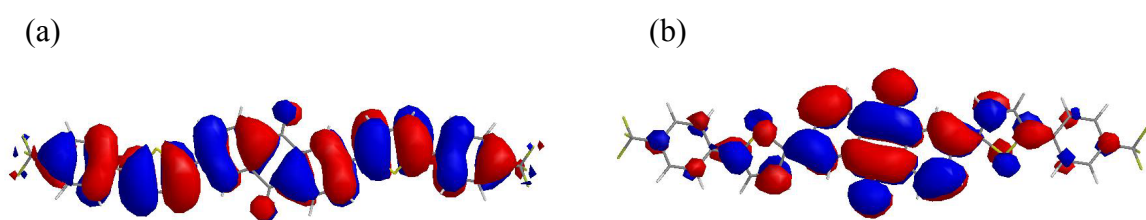


Figure S5. (a) HOMO orbital (-6.25 eV) and (b) LUMO orbital (-3.25 eV) of **2**.

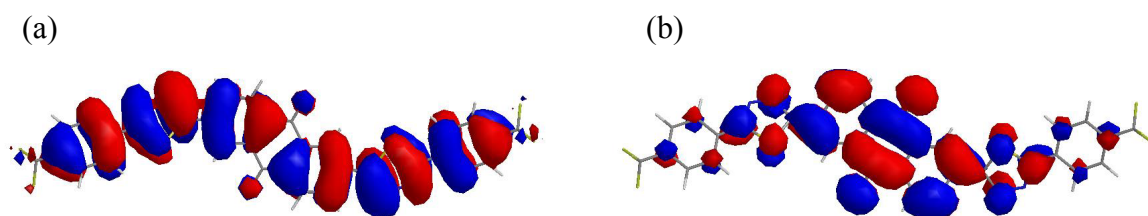


Figure S6. (a) HOMO orbital (-6.53 eV) and (b) LUMO orbital (-3.43 eV) of **3**.

5. X-ray analyses

The measurements were carried out on a Rigaku RAXIS-RAPID Imaging Plate diffractometer (Mo-K α radiation, $\lambda = 0.71075 \text{ \AA}$). The data were collected at 93 K and the structures were solved by the direct method (SIR97) and expanded using Fourier techniques. The non-hydrogen atoms were refined anisotropically. Hydrogen atoms were refined using the riding model.

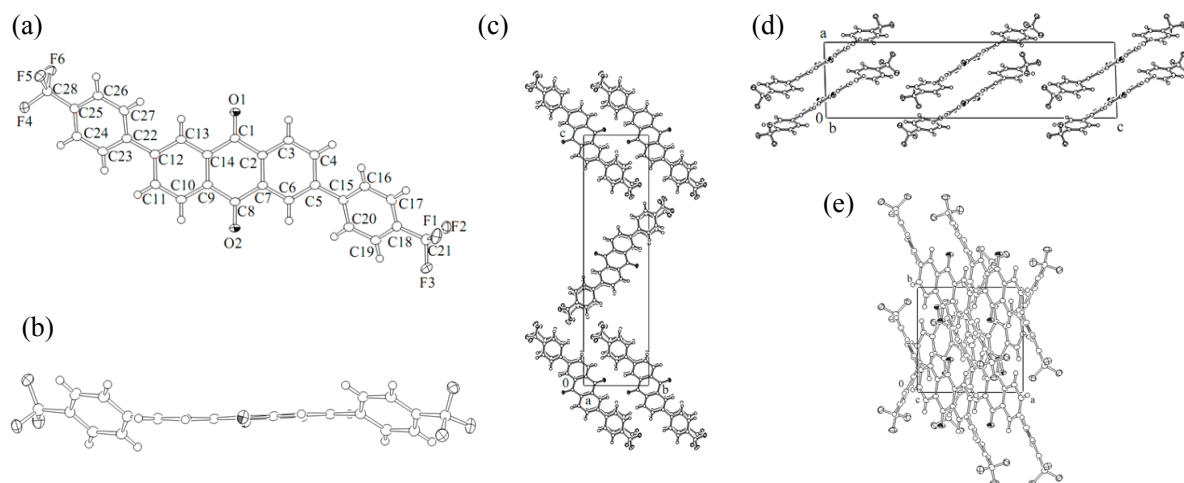


Figure S7. (a) Front view and (b) side view of **1**. (c) The packing of **1** as seen down the *a*-axis projection. (d) *b*-axis projection. (e) *c*-axis projection.

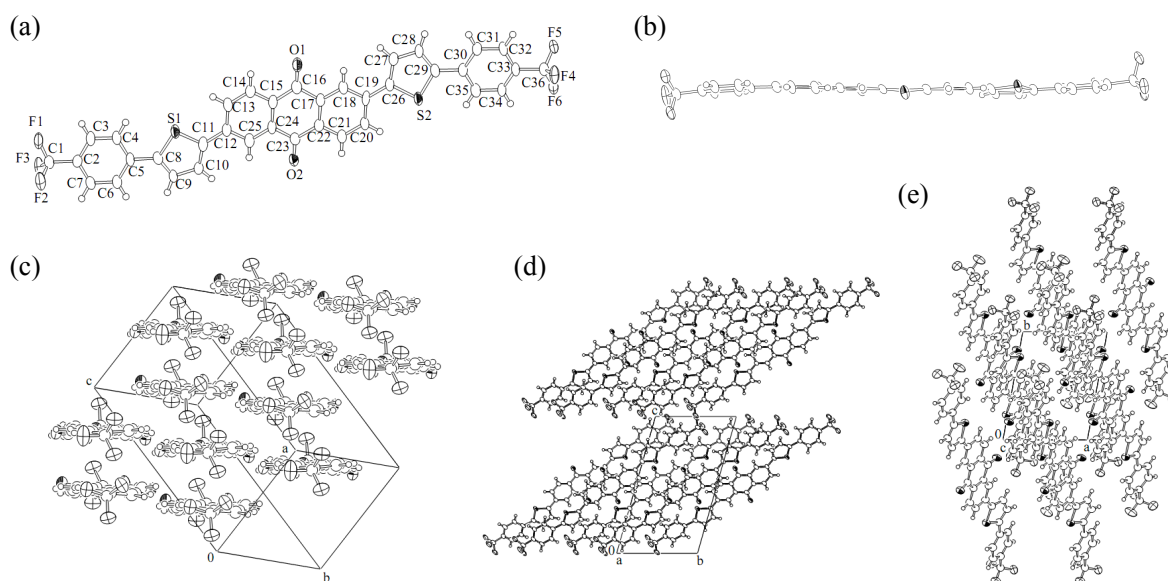


Figure S8. (a) Front view and (b) side view of **2**. (c) The packing in **2** as seen down the long molecular axis. (d) *a*-axis projection. (e) *c*-axis projection.

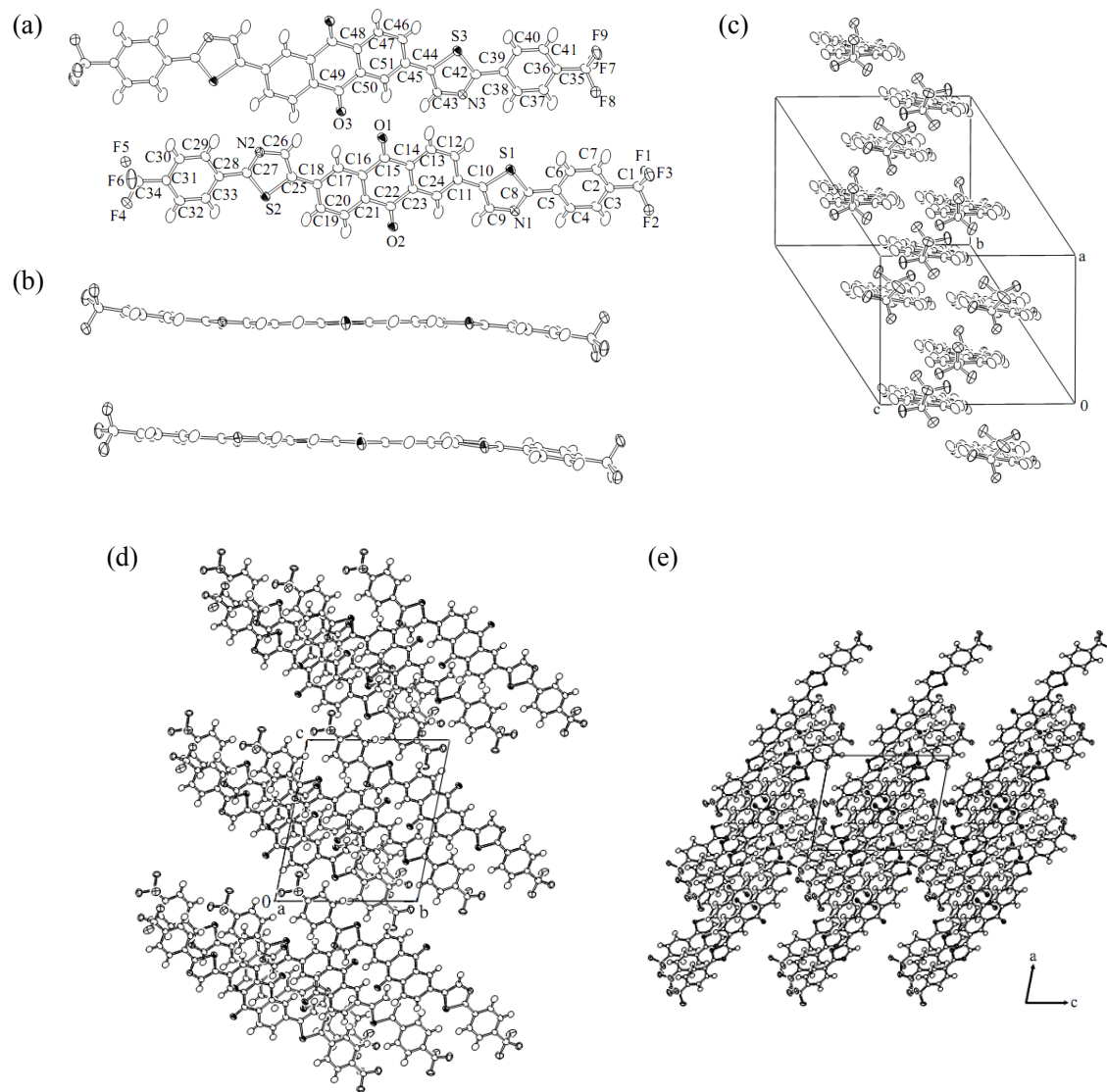


Figure S9. (a) Front view and (b) side view of **3**. (c) The packing in **3** as seen down the long molecular axis.
(d) *a*-Axis projection. (e) *b*-Axis projection.

6. XRD patterns

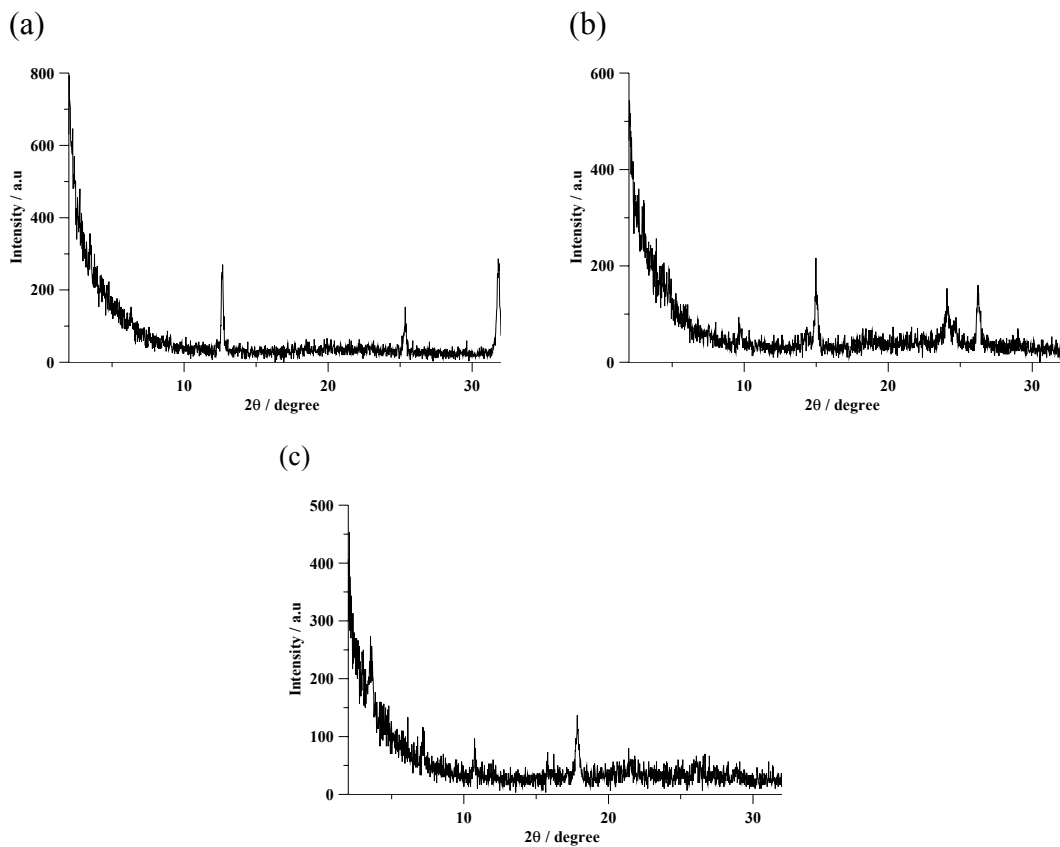


Figure S10. X-ray diffractograms of 50 nm films (a) for **1**, (b) for **2** and (c) for **3** deposited at 50 °C on untreated substrate.

7. AFM measurements

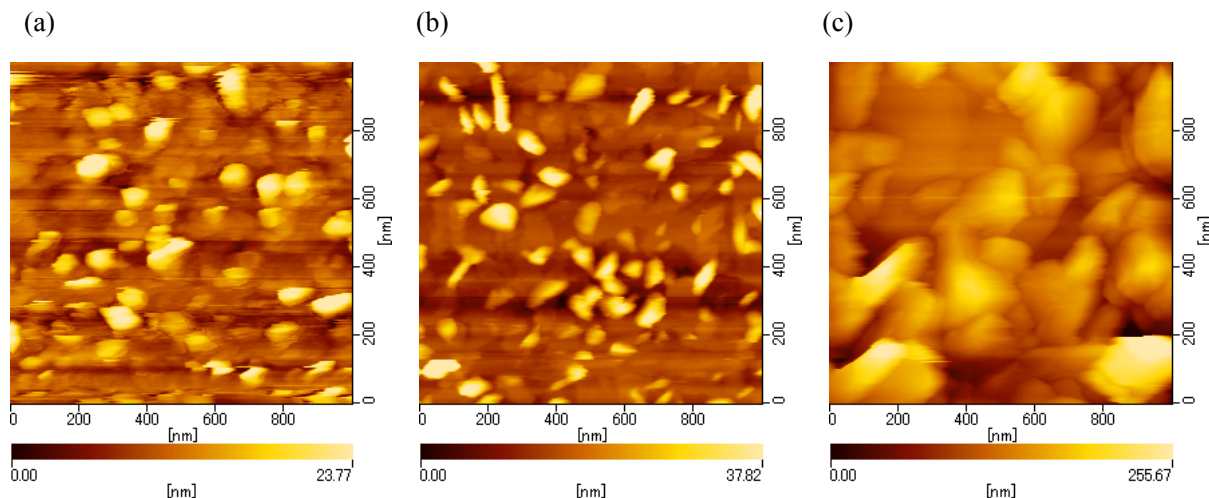


Figure S11. AFM images of **3** deposited at 50 °C. (a) 30 nm film on untreated substrate. (b) 30 nm film on HMDS-treated substrate. (c) 50 nm film on untreated substrate.

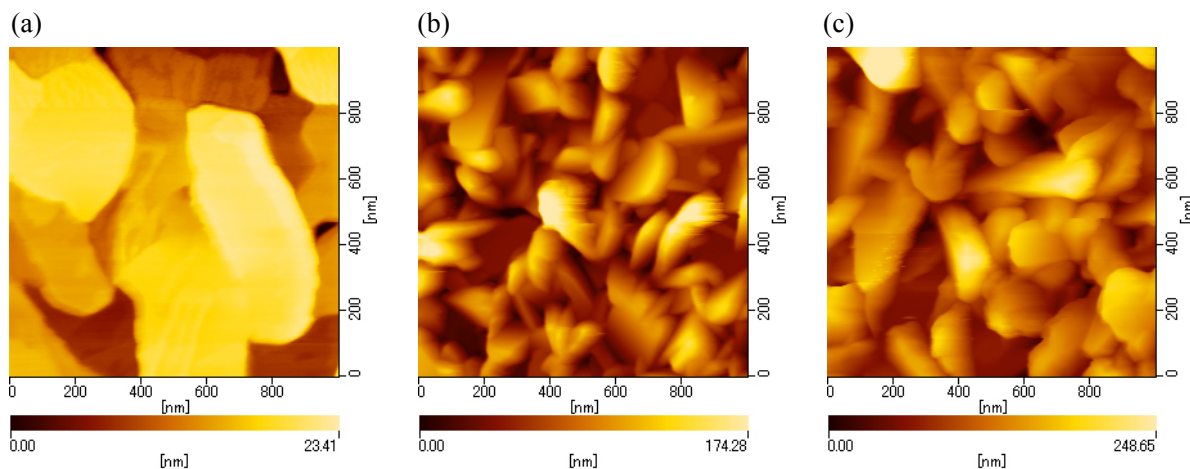


Figure S12. AFM images of 50 nm films (a) for **1**, (b) for **2** and (c) for **3** deposited at 50 °C on HMDS-treated substrate.

8. Device fabrications

The HMDS (hexamethyldisilazane) treatment was carried out by immersing the substrate in HMDS at room temperature for 12–48 h. OFETs were constructed on heavily doped n-type silicon wafers covered with thermally grown silicon dioxide. The silicon dioxide acts as a gate dielectric layer, and the silicon wafer serves as a gate electrode. Several types of devices which have different configurations, or channel length (L) and width (W) were fabricated.

Bottom contact electrodes; The SiO_2 gate dielectric was 300 nm thick. The source and drain electrodes were Cr (10 nm)/Au (20 nm). L/W are 50/294000 μm or 50/500 μm . Organic semiconductors (500 Å) were deposited on the channel region by vacuum evaporation at a rate of 0.2–0.3 Å s⁻¹ under pressure of 10⁻⁵ Pa. During the evaporation, the temperature of the substrate was maintained to 50 °C..

Top contact electrodes; The SiO_2 gate dielectric was 200 nm thick. Organic semiconductors (300 Å) were deposited on the silicon dioxide by vacuum evaporation at a rate of 0.2 Å s⁻¹ under pressure of 10⁻⁵ Pa. During the evaporation, the temperature of the substrate was maintained to 50 °C by heating a copper block on which the substrate was mounted. Gold was used as source and drain electrodes and deposited on the organic semiconductor layer through a shadow mask with $L/W = 50/1000 \mu\text{m}$, 100/1000 μm , 150/1000 μm or 200/1000 μm .

The FET measurements were carried out at room temperature in a vacuum chamber (10⁻⁵ Pa) without exposure to air with Hewlett-Packard 4140A and 4140B models. Under air, the FET performances were not observed.

Mobilities (μ) were calculated in the saturation regime by the relationship: $\mu_{\text{sat}} = (2I_D)/[WC_{\text{ox}}(V_G - V_{\text{th}})^2]$ where I_D is the source-drain saturation current; C_{ox} (4 F) is the oxide capacitance; V_G is the gate voltage and V_{th} is the threshold voltage. The latter can be estimated as the intercept of the linear section of the plot of $V_G (I_D)^{1/2}$

9. FET characteristics

Table S1 FET characteristics of **1**, **2** and **3**-based bottom contact devices

Compound	T_{sub} (°C)	Surface treatment	Mobility ($\text{cm}^2\text{V}^{-1}\text{s}^{-1}$)	On/off ratio	Threshold (V)
1^a	rt	Bare	5.6×10^{-4}	3×10^4	39
	rt	HMDS	3.6×10^{-4}	5×10^3	38
	50	Bare	1.4×10^{-4}	7×10^3	39
	50	HMDS	7.0×10^{-4}	7×10^4	37
2^b	rt	Bare	0.022	4×10^3	24
	rt	HMDS	0.012	1×10^3	26
	50	Bare	0.020	2×10^3	24
	50	HMDS	0.020	6×10^2	26
3^b	rt	Bare	0.053	6×10^3	19
	rt	HMDS	0.061	3×10^3	25
	50	Bare	0.088	4×10^3	20
	50	HMDS	0.074	1×10^4	25

^aSiO₂ : 300 nm, L/W = 50/294000, S/D electrodes : Cr(10 nm)/Au(20 nm)

^bSiO₂ : 300 nm, L/W = 50/500, S/D electrodes : Cr(10 nm)/Au(20 nm)

Table S2 FET characteristics of **1**, **2** and **3**-based top contact devices

Compound	T_{sub} (°C)	Surface treatment	Mobility ($\text{cm}^2\text{V}^{-1}\text{s}^{-1}$)	On/off ratio	Threshold (V)
1	50	Bare	5.7×10^{-5}	1×10^2	33
	50	HMDS	1.2×10^{-4}	2×10^2	32
2	50	Bare	5.7×10^{-5}	1×10^2	21
	50	HMDS	0.0049	1×10^4	26
3	rt	Bare	8.7×10^{-5}	7×10^2	6
	rt	HMDS	0.038	2×10^5	21
	50	Bare	0.0072	2×10^4	20
	50	HMDS	0.067	3×10^5	21

SiO₂ : 200 nm, L/W = 50/1000, S/D electrodes : Au(50 nm)

10. I_D - V_D and I_D - V_G characteristics

10-1. Bottom contact devices

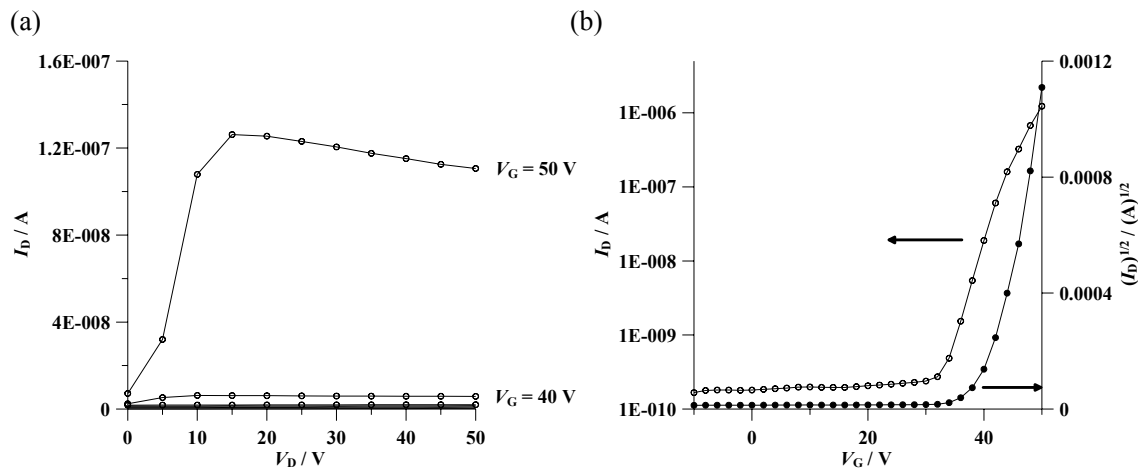


Figure S13. (a) Output characteristics of **1** and (b) Transfer characteristics of **1** at a drain voltage of 50 V ($T_{\text{sub}} = 50$ °C, Bare). The mobility calculated in the saturation regime is 1.4×10^{-4} cm 2 V $^{-1}$ s $^{-1}$.

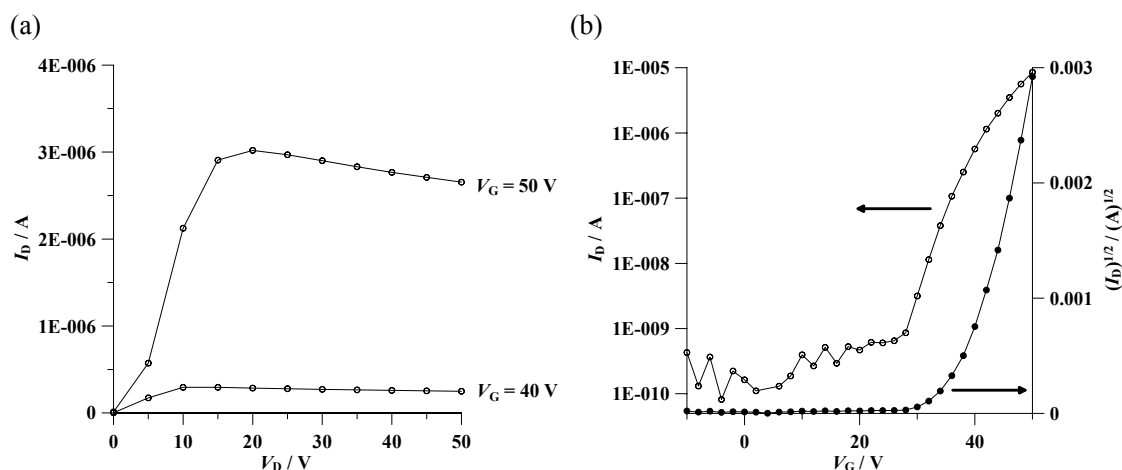


Figure S14. (a) Output characteristics of **1** and (b) Transfer characteristics of **1** at a drain voltage of 50 V ($T_{\text{sub}} = 50$ °C, HMDS). The mobility calculated in the saturation regime is 7.0×10^{-4} cm 2 V $^{-1}$ s $^{-1}$.

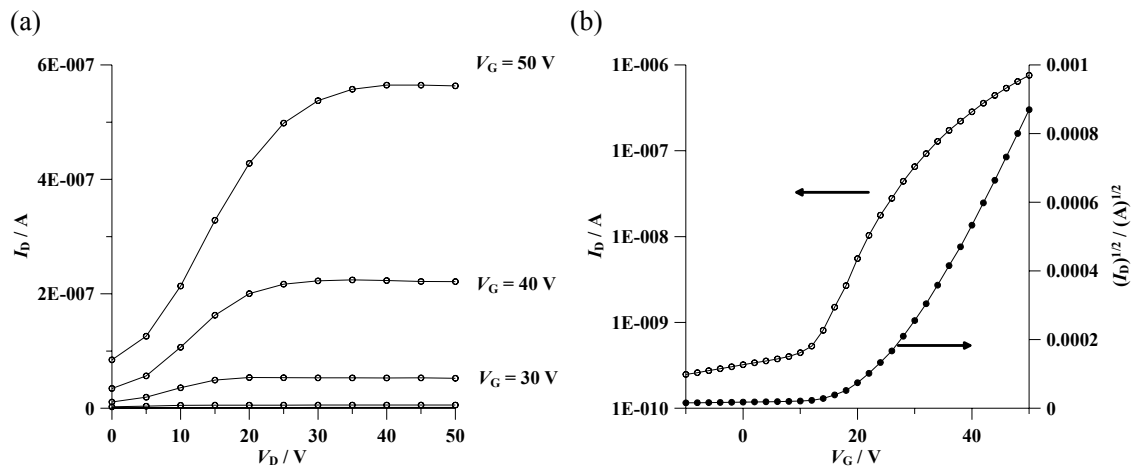


Figure S15. (a) Output characteristics of **2** and (b) Transfer characteristics of **2** at a drain voltage of 50 V ($T_{\text{sub}} = 50^\circ\text{C}$, Bare). The mobility calculated in the saturation regime is $0.020 \text{ cm}^2 \text{ V}^{-1} \text{ s}^{-1}$.

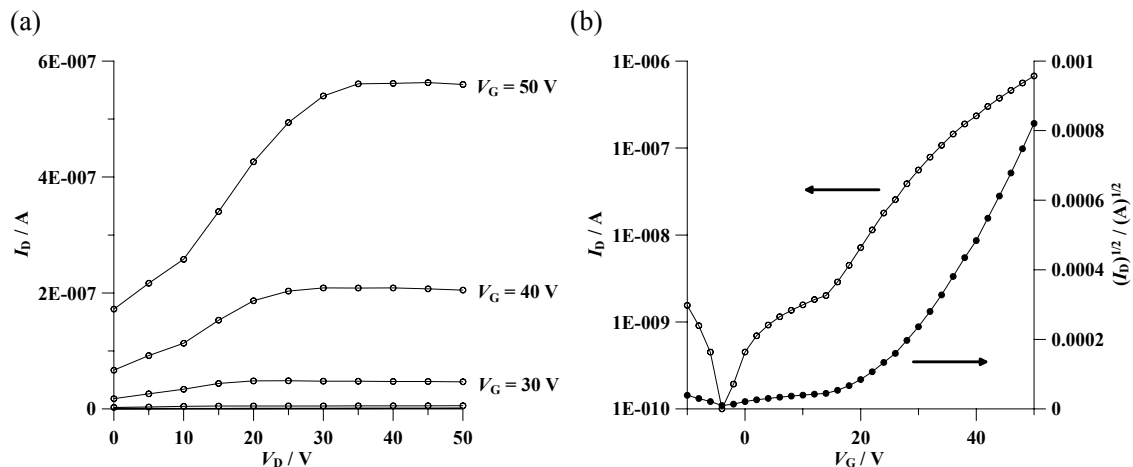


Figure S16. (a) Output characteristics of **2** and (b) Transfer characteristics of **2** at a drain voltage of 50 V ($T_{\text{sub}} = 50^\circ\text{C}$, HMDS). The mobility calculated in the saturation regime is $0.020 \text{ cm}^2 \text{ V}^{-1} \text{ s}^{-1}$.

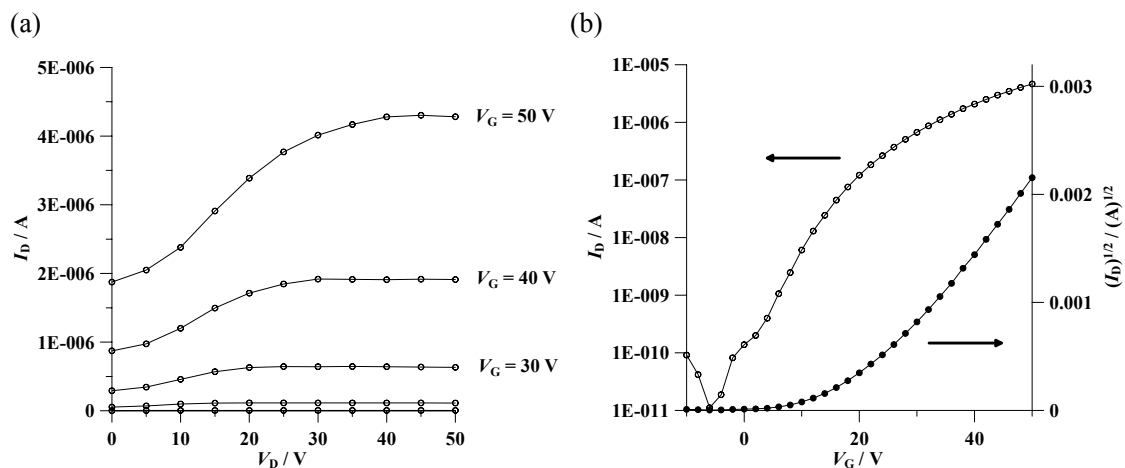


Figure S17. (a) Output characteristics of **3** and (b) Transfer characteristics of **3** at a drain voltage of 50 V ($T_{\text{sub}} = 50^\circ\text{C}$, Bare). The mobility calculated in the saturation regime is $0.088 \text{ cm}^2 \text{ V}^{-1} \text{ s}^{-1}$.

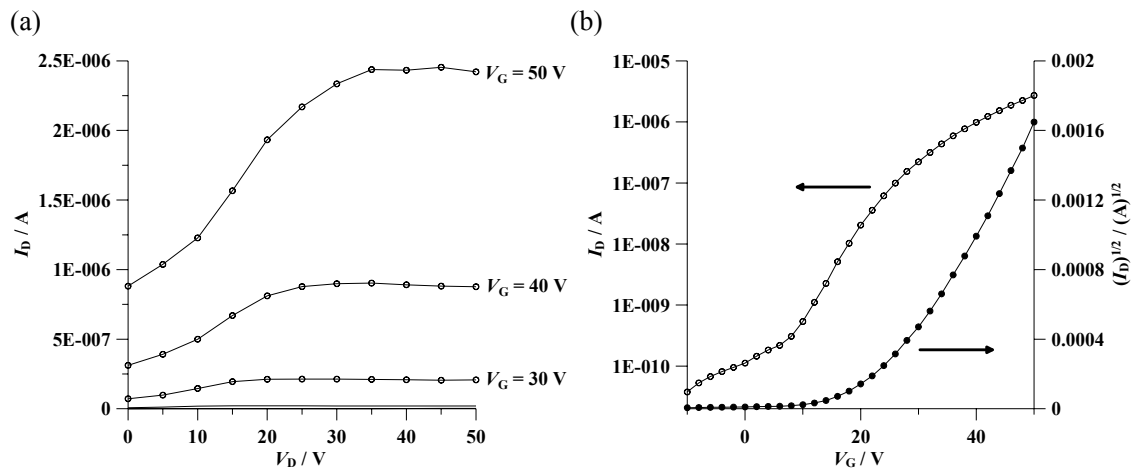


Figure S18. (a) Output characteristics of **3** and (b) Transfer characteristics of **3** at a drain voltage of 50 V ($T_{\text{sub}} = 50$ °C, HMDS). The mobility calculated in the saturation regime is $0.074 \text{ cm}^2 \text{ V}^{-1} \text{ s}^{-1}$.

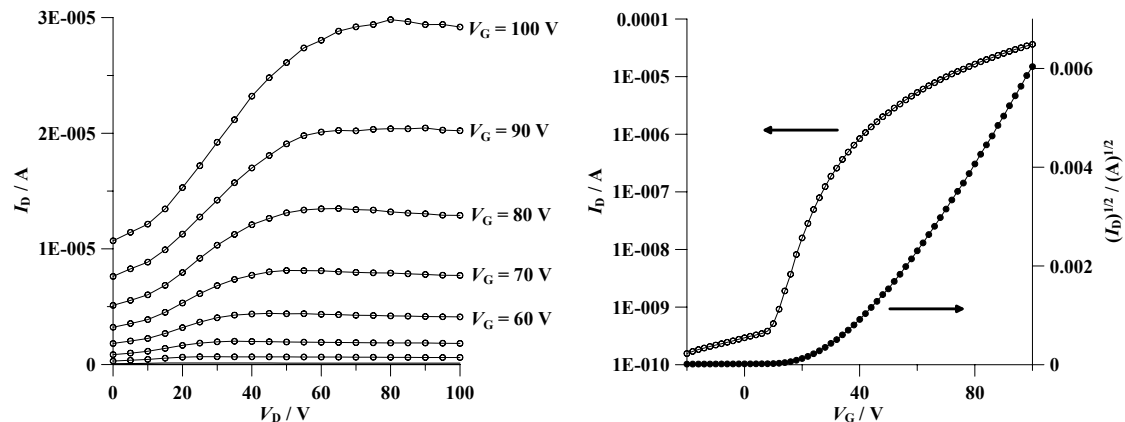


Figure S19. (a) Output characteristics of **3** and (b) Transfer characteristics of **3** at a drain voltage of 100 V ($T_{\text{sub}} = 50$ °C, HMDS). The mobility calculated in the saturation regime is $0.18 \text{ cm}^2 \text{ V}^{-1} \text{ s}^{-1}$.

10-2. Top contact devices

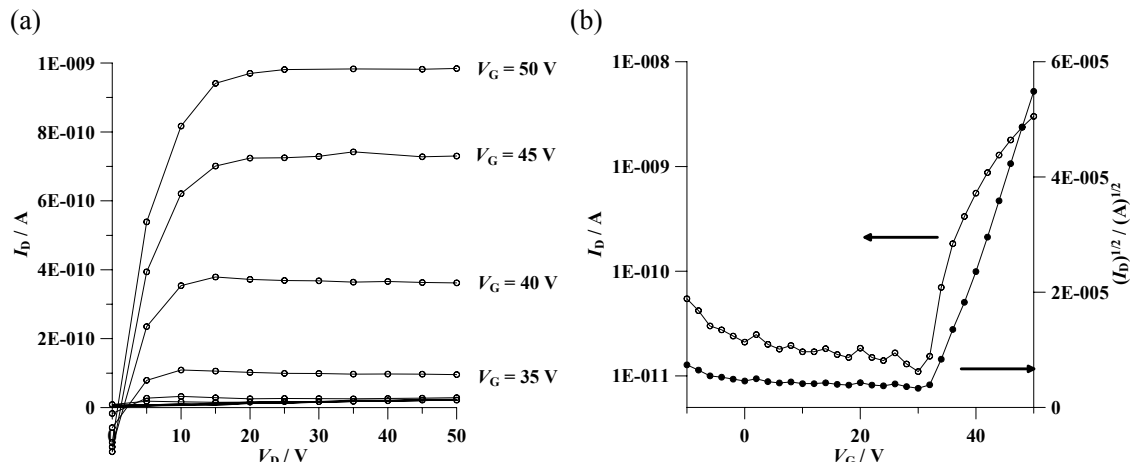


Figure S20. (a) Output characteristics of **1** and (b) Transfer characteristics of **1** at a drain voltage of 50 V ($T_{\text{sub}} = 50$ °C, Bare). The mobility calculated in the saturation regime is $5.7 \times 10^{-5} \text{ cm}^2 \text{ V}^{-1} \text{ s}^{-1}$.

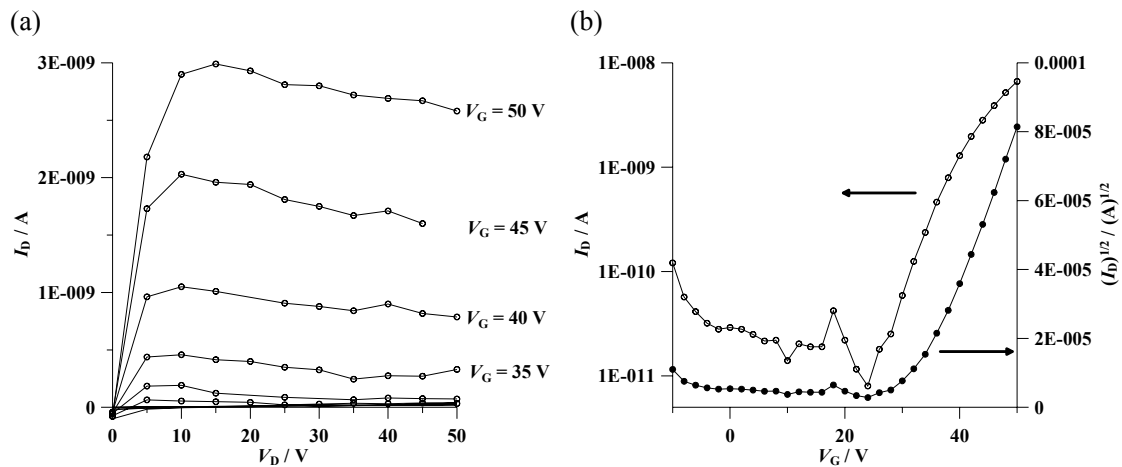


Figure S21. (a) Output characteristics of **1** and (b) Transfer characteristics of **1** at a drain voltage of 50 V ($T_{\text{sub}} = 50^\circ\text{C}$, HMDS). The mobility calculated in the saturation regime is $1.2 \times 10^{-4} \text{ cm}^2 \text{ V}^{-1} \text{ s}^{-1}$.

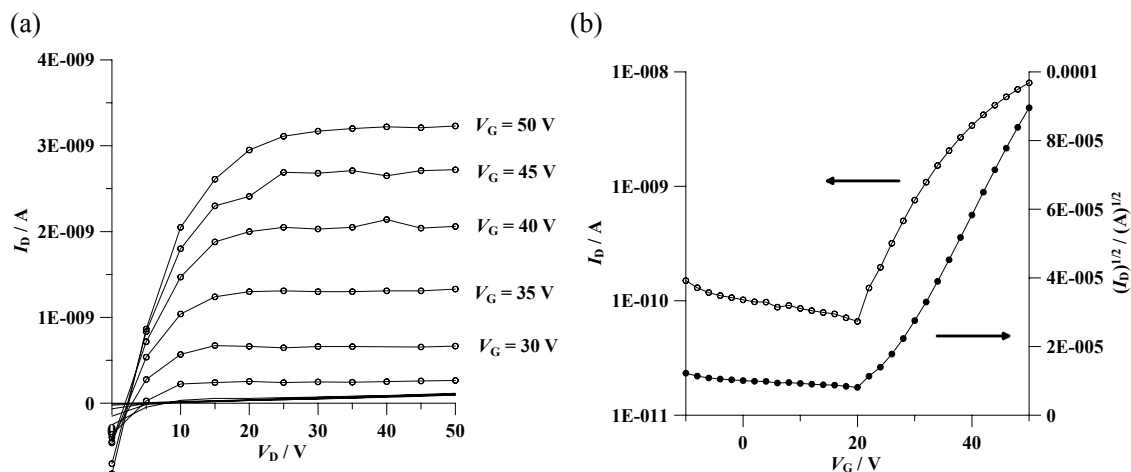


Figure S22. (a) Output characteristics of **2** and (b) Transfer characteristics of **2** at a drain voltage of 50 V ($T_{\text{sub}} = 50^\circ\text{C}$, Bare). The mobility calculated in the saturation regime is $5.7 \times 10^{-5} \text{ cm}^2 \text{ V}^{-1} \text{ s}^{-1}$.

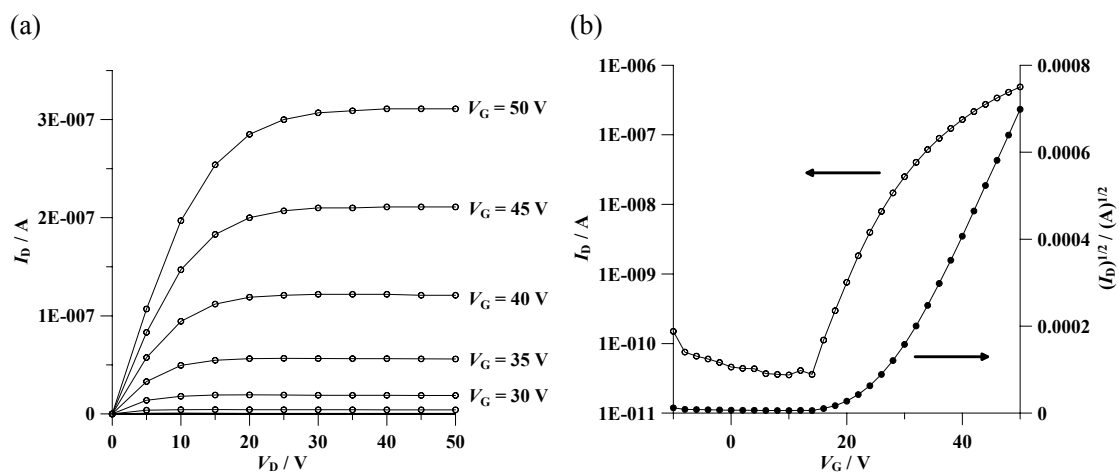


Figure S23. (a) Output characteristics of **2** and (b) Transfer characteristics of **2** at a drain voltage of 50 V ($T_{\text{sub}} = 50^\circ\text{C}$, HMDS). The mobility calculated in the saturation regime is $0.0049 \text{ cm}^2 \text{ V}^{-1} \text{ s}^{-1}$.

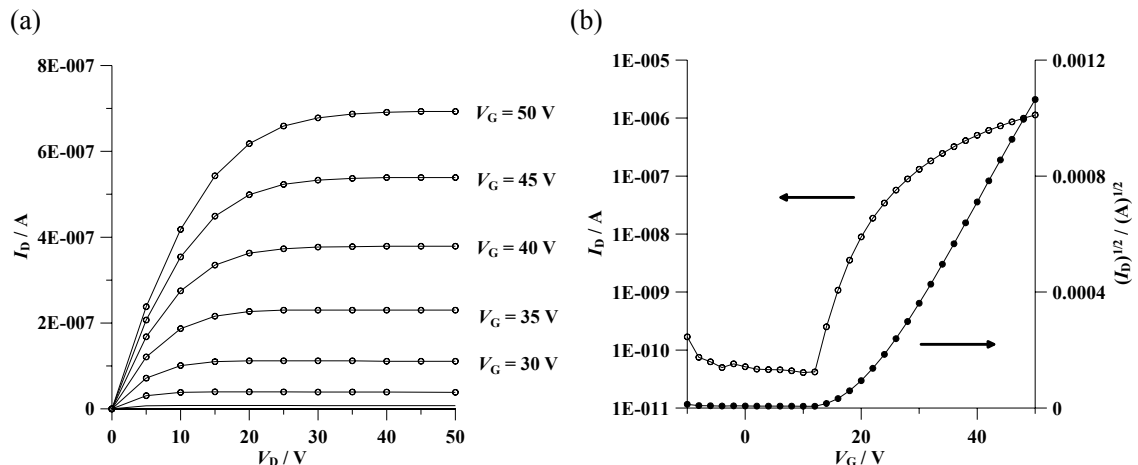


Figure S24. (a) Output characteristics of **3** and (b) Transfer characteristics of **3** at a drain voltage of 50 V ($T_{\text{sub}} = 50^\circ\text{C}$, Bare). The mobility calculated in the saturation regime is $0.0072 \text{ cm}^2 \text{ V}^{-1} \text{ s}^{-1}$.

11. References

- 1 S. K. Lee, W. J. Yang, J. J. Choi, C. H. Kim, S.-J. Jeon, and B. R. Cho, *Org. Lett.* **2005**, *7*, 323.
- 2 J. Morgan and J. T. Pinhey, *J. Chem. Soc., Perkin Trans. I* **1990**, 715.
- 3 M. Mamada, J. Nishida, D. Kumaki, S. Tokito, and Y. Yamashita, *Chem. Mater.* **2007**, *19*, 5404.